# A Virtual Complex Impedance Based $P-\dot{V}$ Droop Method for Parallel-Connected Inverters in Low-Voltage AC Microgrids

Jianbo Chen, *Student Member, IEEE*, Dong Yue, *Senior Member, IEEE*, Chunxia Dou, *Member, IEEE*, Lei Chen, *Student Member, IEEE*, Shengxuan Weng, and Yanman Li

***Abstract*—Due to the high R/X ratio and mismatched feeder impedance of low-voltage microgrids, conventional droop method is no longer able to decouple the active and reactive power of distributed generators and the power-sharing accuracy is degraded. In this article, a virtual complex impedance based $P-\dot{V}$ droop method is proposed to decouple the powers and improve the power-sharing accuracy among DGs. With the virtual impedance method, the equivalent impedance between virtual power source and point of common coupling is shaped to be purely resistive. Then, a $P-\dot{V}$ strategy is adopted to alleviate the effect of mismatched line impedance, where the virtual powers rather than the ordinary *P/Q* are used in the droop equation. In case the output voltage violates the operation code, a restoration mechanism is proposed to reset $\dot{V}$ to zero. Compared with existing virtual impedance and $Q-\dot{V}$ droop methods, the proposed method combines the advantages of both. Besides, a modified $P-\dot{V}$ strategy is also presented to accelerate the restoration process and improve the active power-sharing accuracy at the same time. Simulation results validate the effectiveness of the proposed method.**

***Index Terms*—Droop control, low-voltage ac microgrid, power-sharing, virtual impedance.**

## I. Introduction

RENEWABLE energy, such as solar and wind power, is seen as an appropriate solution to sustainable development and is often integrated into utility grid through distributed generators (DGs). To incorporate and coordinate different types of DGs, the microgrid (MG) which can operate in both grid-connected and islanded modes has emerged and has been widely accepted [1]–[5].

In the islanded operation of the MG, the DGs are controlled as voltage sources and parallel connected through the MG. To ensure stability of the MG, the active and reactive powers of the DGs should be shared simultaneously [6]. Besides, each DG should be able to operate independently without communication for the practical and economic concerns. Therefore, the droop control method, which mimics the behavior of synchronous generators, has been extensively adopted in MG for its ability of fulfilling the aforementioned requirements [5]–[8].

The conventional droop control methods were proposed for purely inductive feeder impedance. In this scenario, the frequency is a global quantity and thus the active power can be shared accurately. On the contrary, the voltage magnitude profile is deeply influenced by mismatched feeder impedance and the reactive power-sharing accuracy is often degraded [5]. To improve the reactive power-sharing accuracy, various modified droop methods have been proposed and can be roughly divided into two categories [9]: open-loop [10]–[16] and closed-loop [17]–[23]. The closed-loop reactive power-sharing methods can be further divided into the following: Small signal injection [17]–[19], detection of voltage of point of common coupling (PCC) [20], [21], detection of load change [22], and compensation of impedance voltage drop [23]. The small signal injection method [17],[19] requires a small ac voltage signal added into the output voltage reference, which may reduce the quality of the output voltage and current. Besides, the extraction and process of the small signal increase the complexity of the physical realization. Since the DGs may be installed dispersedly, the detection of voltage of PCC [20], [21] is impractical in this situation. In [22], wavelet transform is adopted to detect the load change, which increases the complexity of the controller. In [23], with estimation of impedance voltage drop effect and compensation of the local load, the output power is shared accurately in both grid-connected and islanded mode. However, the islanded sharing accuracy is dependent on the operation of grid-connected mode in advance.

Compared with the closed-loop methods, open-loop schemes are easier to be implemented in actual MG systems [9]. In general, the open-loop strategies can be classified into two types: Virtual impedance [10]–[14] and $Q-\dot{V}$ method [15], [16]. The original idea of virtual impedance strategy is to incorporate

Manuscript received January 6, 2020; revised March 26, 2020; accepted May 18, 2020. Date of publication May 25, 2020; date of current version November 20, 2020. This work was supported by the National Natural Science Foundation of China under Grant 61533010, Grant 61833008, and Grant 61933005. Paper no. TII-20-0076. *(Corresponding authors: Dong Yue; Chunxia Dou.)*

Jianbo Chen, Dong Yue, Chunxia Dou, Lei Chen, and Shengxuan Weng are with the Institute of Advanced Technology, Nanjing University of Posts and Telecommunications, Nanjing 210023, China (e-mail: jianbo686@aliyun.com; medongy@vip.163.com; cxdou@ysu.edu.cn; cchlorine@163.com; shxweng@gmail.com).

Yanman Li is with the NARI Technology Co., Ltd, Nanjing 211000, China (e-mail: liyanman@sgepri.sgcc.com.cn).

Color versions of one or more of the figures in this article are available online at https://ieeexplore.ieee.org.

Digital Object Identifier 10.1109/TII.2020.2997054

a virtual impedance to reshape the output impedance of DGs to be purely inductive or resistive. Therefore, the active and reactive power is decoupled and can be controlled independently. Besides, the virtual impedance does not introduce extra power losses, which is also an appealing advantage. In [10], virtual negative resistance and inductance is adopted to reshape the equivalent impedance between virtual power source (VPS) and PCC to be purely inductive. With proper selection of virtual inductance, the accurate reactive power-sharing is achieved. In [11], an adaptive virtual output impedance is constructed such that the impedance at fundamental frequency is inductive while resistive at harmonic orders. Hence, not only the active and reactive power but also the harmonic power is shared accurately. However, the mismatch of the feeder impedance, including transformers, cables and the grid-side inductors, is not considered [24].

Differing from the virtual impedance based methods, a novel $Q - \dot{V}$ droop method is proposed in [15] and [25] to improve the reactive power-sharing accuracy without modifying the output impedance and a $\dot{V}$ restoration mechanism is adopted to reset $\dot{V}$ to zero at steady state. Since the restoration process of different DGs will never be the same [26], the set point of DGs will be different. Thus, the $Q - \dot{V}$ droop method is not able to tackle the power-sharing performance thoroughly. To address the set point deviation problem based on local information only, a modified $\dot{V}$ restoration technique was proposed in [16] to reduce the deviation of $Q_{0x}$ before entering the steady state. Despite the effectiveness of the $Q - \dot{V}$ method under purely inductive cases, its performance is degraded when the equivalent impedance is complex, since the active and reactive power are affected by both voltage magnitude and phase difference.

As for low-voltage microgrids (LVMGs) where feeder impedance is mainly resistive, extensive works have been done to reshape the output impedance to be purely inductive [10]–[19], [21]–[24] based on the assumption that the output impedance of DG is inductive and larger value of grid-side inductor is adopted. However, this assumption is not always true since the output impedance mainly depends on the control strategy [27] and the grid-side inductor may be small when LCL is designed for active power filter. Compared with purely inductive cases, few attention has been paid to purely resistive case [27],[28]. In [27], the output impedance of parallel DGs is shaped to be resistive, where the $Q - \dot{V}$ droop equation is replaced by the $P - \dot{V}$ droop control equation. With the resistive output impedance, the overall system is more damped and the harmonic current is automatically shared [28]. However, the mismatch of feeder impedance is still ignored the same as in [11] which will have great limitations in real applications.

In view of extensive purely inductive cases and lack of more practical solutions for resistive scenarios, an open-loop method which can not only improve the active power-sharing accuracy but also easier to be implemented in low-cost microcontrollers is required. Comparing the virtual impedance strategy with $Q - \dot{V}$ droop method, it is concluded that the former is a powerful tool to decouple the active and reactive power with limited ability to compensate the mismatch of feeder impedance while the latter

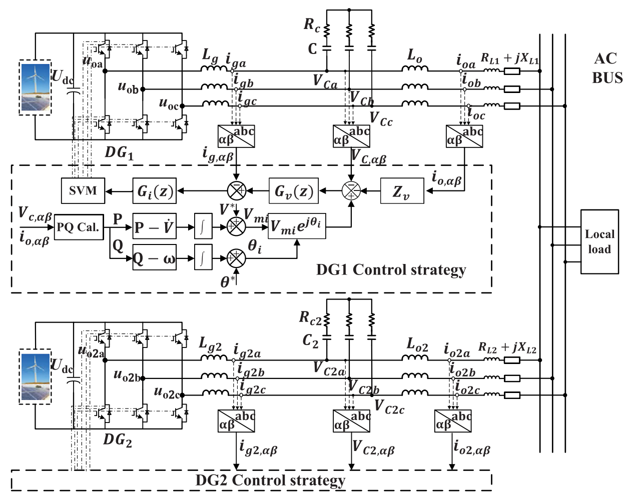


Fig. 1. Configuration of the investigated MG.

is better at reducing the effect of mismatched line impedance without consideration of power coupling.

Therefore, in this article, a virtual complex impedance based $P - \dot{V}$ droop method which combines the advantages of both virtual impedance based method [27] and $Q - \dot{V}$ droop method [15] is proposed to solve the power-sharing problem of LVMG. Besides, in most existing papers, $P$ and $Q$ adopted in droop equations are calculated according to the capacitor voltage and grid-side current, which are not actually decoupled since the physical impedance between PCC and filter capacitor is still complex. The actually decoupled *P/Q* injected by VPS is adopted in this article, since the impedance between PCC and VPS is reshaped to be purely resistive. In addition to the original $P - \dot{V}$ droop method, a modified $P - \dot{V}$ method is also proposed, where an extra parameter $S_p$ is utilized to accelerate the dynamic regulation performance and active power-sharing accuracy at the same time.

The remainder of this article is organized as follows. In Section II, system modeling and controller design are presented at first. Then, the virtual complex impedance strategy is adopted to reshape the equivalent impedance. Section III describes the proposed original and modified $P - \dot{V}$ method, where a restoration mechanism is also incorporated. Section IV discusses the effects of control parameters and Section V presents the simulation results. Finally, Section VI concludes this article.

## II. Islanded Microgrid Structure, Modeling, and Control

In this study, two parallel-connected DGs with LCL filters are analyzed, where the passive damping method is taken for robustness, as shown in Fig. 1. Besides, the dc voltage is considered as constant for simplicity. The local balanced load consisting of resistors and inductors is shared by the two DGs. To analyze the influence of mismatched feeder impedance, the line impedance is set to be different. The detailed analysis of the control loop is presented as follows.

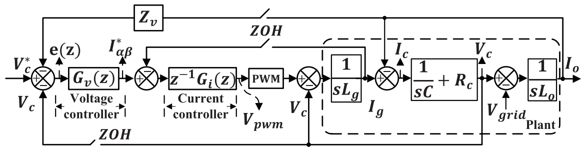


Fig. 2. Inner control loop.

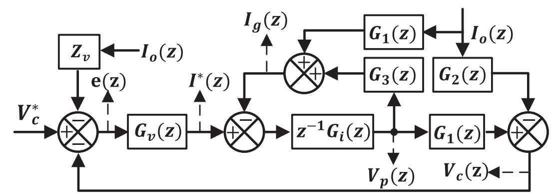


Fig. 3. Inner control loop in $z$-domain.

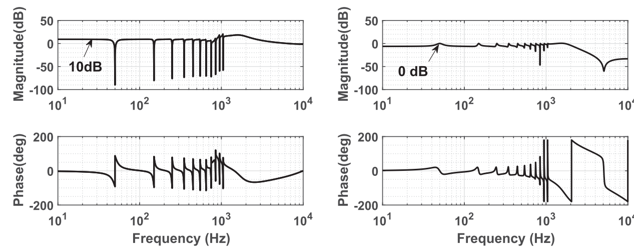


(a) (b)

Fig. 4. Bode plot of (a) $Z_o(z)$ and (b) $G_4(z)$.

## A. Voltage and Current Control Loop in Stationary Frame

The detailed block diagram of the inner loop is shown as in Fig. 2, where proportional resonant (PR) controller is adopted in the outer voltage control loop while *P* controller is preferred in the inner current control loop. $z^{-1}$ is incorporated to model the computation delay. Besides, the resistor parasitics of DG and grid-side inductor are ignored for the most unstable cases.

The discrete formulation of PR controller is shown as [29], [30]

$$G_v(z) = G_{PR}(z) = K_p + K_i \cdot R_{tp}(z) \tag{1}$$

where $K_p$ is the proportional coefficient and $K_i$ is the resonant one, and

$$\begin{aligned} R_{tp}(z) = &\frac{0.5(1-z^{-2})\cos(\varphi)\sin(\omega_e T_s)}{\omega_e(1-2z^{-1}\cos(\omega_e T_s)+z^{-2})} \\ &- \frac{(1+2z^{-1}+z^{-2})\sin(\varphi)\left\{\sin\frac{\omega_e T_s}{2}\right\}^2}{\omega_e(1-2z^{-1}\cos(\omega_e T_s)+z^{-2})} \end{aligned} \tag{2}$$

where $T_s$ is the sampling rate, $\varphi$ is the leading angle which should be properly designed to compensate for the delay of controlled plant, $\omega_e$ is the controlled frequency, which is equal to the angular frequency derived by droop equation.

The proportional term $G_i(z) = K_I$ is suitable for the inner current controller to provide extra virtual damping for the LCL filter and the PCC voltage is seen as disturbance. Then, according to Fig. 2, the following equation is derived:

$$\begin{cases} (V_{\rm pwm}(s) - V_c(s))\,\frac{1}{sL_g} = I_g \\ (I_g(s) - I_o(s))\left(\frac{1}{sC} + R_c\right) = V_c(s) \end{cases} \tag{3}$$

where $V_{\rm pwm}$ is the modulated voltage reference while $V_c$ is the capacitor voltage, $L_g$ is the inverter-side inductor, $I_g$ and $I_o$ are the inverter-side and grid-side current, $C$ is the filter capacitor, and $R_c$ is the resistor used for passive damping.

From (3), the following formulation is derived:

$$\begin{cases} V_c(s) = G_1(s)V_p(s) - G_2(s)I_o(s) \\ I_g(s) = G_3(s)V_p(s) + G_1(s)I_o(s) \end{cases} \tag{4}$$

where $V_{\rm pwm}$ is simply denoted as $V_p$ and $G_1(s) = \frac{sCR_c+1}{s^2L_gC+sCR_c+1}$, $G_2(s) = \frac{s^2L_gCR_c+sL_g}{s^2L_gC+sCR_c+1}$, and $G_3(s) = \frac{sC}{s^2L_gC+sCR_c+1}$.

Considering the characteristic of zero-hold, $G_{1,2,3}(s)$ are discretized as [29]

$$\begin{aligned} G_1(z) = &\frac{e^{-2aT_s} + z - (z+1)e^{-aT_s}\cos(\omega_r T_s)}{z^2 - 2ze^{-aT_s}\cos(\omega_r T_s) + e^{-2aT_s}} \\ &+ \frac{\frac{R_c(z-1)}{2L_g\omega_r}(z-1)e^{-aT_s}\sin(w_r T_s)}{z^2 - 2ze^{-aT_s}\cos(\omega_r T_s) + e^{-2aT_s}} \end{aligned}$$

$$\begin{aligned} G_2(z) = &\frac{R_c(z-1)(z - e^{-aT_s}\cos(\omega_r T_s))}{z^2 - 2ze^{-aT_s}\cos(\omega_r T_s) + e^{-2aT_s}} \\ &+ \frac{\frac{2L_g - R_c^2 C}{2L_g C\omega_r}(z-1)e^{-aT_s}\sin(\omega_r T_s)}{z^2 - 2ze^{-aT_s}\cos(\omega_r T_s) + e^{-2aT_s}} \\ G_3(z) = &\frac{(z-1)e^{-aT_s}\sin(\omega_r T_s)}{z^2 - 2ze^{-aT_s}\cos(\omega_r T_s) + e^{-2aT_s}} \cdot \frac{1}{\omega_r L_g} \end{aligned} \tag{5}$$

where $a = \frac{R_c}{2L_g}, \omega_r = \sqrt{\frac{1}{L_gC} - \frac{R_c^2}{4L_g^2}}$. Then the block diagram of the inner loop is redrawn as Fig. 3.

According to Fig. 3, the following equation is derived:

$$\begin{cases} [V_c^*(z) - V_c(z)]G_v(z) = I^*(z) \\ [I^*(z) - I_g(z)]G_i(z)z^{-1} = V_p(z) \end{cases}. \tag{6}$$

Combining (4), (5), and (6), one has

$$V_c(z) = G_4(z)V_c^*(z) - Z_o(z)I_o(z) \tag{7}$$

where $G_4(z) = \frac{G_1(z)G_i(z)G_v(z)}{z+G_1(z)G_v(z)G_i(z)+G_3(z)G_i(z)}$, $Z_o(z) = \frac{G_2(z)G_3(z)G_i(z)+G_1^2(z)G_i(z)+zG_2(z)}{z+G_1(z)G_v(z)G_i(z)+G_3(z)G_i(z)}$.

To further investigate the characteristic of the DG, the bode plot of $G_4(z)$ and $Z_o(z)$ is provided in Fig. 4(a) and (b), respectively.

The output impedance of the DGs under the PR controller differs from that under PI controller[11] where the output impedance is nearly inductive at the fundamental frequency. According to Fig. 4(a), the output impedance is nearly resistive (10 dB) around the controlled frequency. The magnitude gain of $Z_o(z)$ at resonant frequencies is negative infinity dB, which means that the output impedance at resonant frequencies is zero. Thus, the output voltage will not be influenced by the output current at resonant frequencies.

Since both the magnitude gain (in dB) and phase gain of $G_4(z)$ are zero at resonant frequencies, as shown in Fig. 4(b),

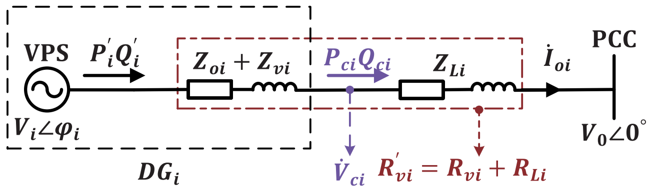


Fig. 5. Equivalent circuit of DG under virtual complex impedance.

the transfer function $G_4(z)$ has no influence on the voltage reference $V_c^*(z)$ at resonant frequencies. Combining the influence of $Z_o(z)$ and $G_4(z)$, the output voltage $V_c(z)$ is able to track the reference $V_c^*(z)$ without steady errors at resonant frequencies.

### B. Virtual Complex Impedance Strategy

Although zero impedance characteristic is an advantage from the aspect of tracking performance, it will exaggerate the circulate current between DGs [31], [32]. Besides, the stability of the system is endangered since the disturbance of output voltage $V_c(z)$ is undamped.

Considering the near resistive characteristic within the controlled frequencies and the effect of grid-side inductors and/or the transformers, the following virtual complex impedance is adopted in this study:

$$Z_{vi} = R_{vi} + \frac{1}{sC_{vi}} = R_{vi} - jX_{vi} \tag{8}$$

where $R_{vi}$ is the virtual resistor and $C_{vi}$ is the virtual capacitor. $X_{vi}$ is the equivalent reactance and $Z_{vi}$ is the virtual complex impedance. Thus, output voltage of DGs is modified as

$$\begin{aligned} V_{ci}(z) &= G_4(z)\left[V_{ci}^*(z) - I_{oi}(z)Z_{vi}\right)] - Z_o(z)I_{oi}(z) \\ &= G_4(z)V_{ci}^*(z) - Z_{oi}^{'}(z)I_{oi}(z) \end{aligned} \tag{9}$$

where $Z_{oi}^{'}(z) = G_4(R_{vi} - jX_{vi}) + Z_o(z)$ is equivalent output impedance.

According to the analysis of Fig. 4(a) and (b), equivalent output impedance is simplified as $Z_{oi}^{'}(z) = Z_{vi} = R_{vi} - jX_{vi}$. The virtual capacitor will alleviate the impact of reactance, especially when the line reactance $X_{Li}$ between DGs and PCC is known or can be estimated. The final impedance $Z_i^{'}$ is reshaped as purely resistive at fundamental frequency as shown in Fig. 5, if $X_{vi}$ is set to be equal to $X_{Li}$

$$\begin{aligned} Z_i^{'} &= Z_{vi} + Z_{Li} = R_{vi} - jX_{vi} + R_{Li} + jX_{Li} \\ &= R_{vi} + R_{Li} = R_{vi}^{'} \end{aligned} \tag{10}$$

where $R_{vi}$ of different DGs is set to be equal, $R_{Li}$ is typically unequal representing the mismatch of feeder impedance, and $R_{vi}^{'}$ is the equivalent impedance between VPS and PCC.

In Fig. 5, $V_i\angle\varphi_i = G_4(z)V_{ci}^*(z)$ is defined as the VPS. $P_i^{'}$ and $Q_i^{'}$ are the virtual active and reactive power injected by $V_i\angle\varphi_i$. $Z_{oi} + Z_{vi}$ is the equivalent output impedance. $Z_{Li}$ is the line impedance. $P_{ci}$ and $Q_{ci}$ is the active and reactive power injected by capacitor voltage $\dot{V}_{ci}$. $V_0\angle 0^{\circ}$ is the PCC voltage. $\dot{I}_i$ is the output current of $DG_i$.

### C. Modified Droop Control Equation

Since the equivalent impedance between VPS and PCC is shaped as purely resistive, the virtual active power $P^{'}$ and reactive power $Q^{'}$ can be expressed as

$$\begin{aligned} P_i^{'} &= \frac{V_i(V_i - V_o)}{R_{vi}^{'}}\cos(\varphi_i) = \frac{V_i(V_i - V_o)}{R_{vi}^{'}} \\ Q_i^{'} &= -\frac{V_iV_o}{R_{vi}^{'}}\sin(\varphi_i) = -\frac{V_iV_o}{R_{vi}^{'}}\varphi_i \end{aligned} \tag{11}$$

where $\varphi_i$ is assumed to be small enough.

Thus, the $P - V$ and $Q - \omega$ droop scheme can be adopted to regulate the frequency and amplitude of the VPS output-voltage reference.

$$\begin{aligned} V_i &= V^* - m_iP_i^{'} \\ \omega_i &= \omega^* + n_iQ_i^{'} \end{aligned} \tag{12}$$

where $m_i$ and $n_i$ are the droop coefficient, $V_i$ and $\omega_i$ are the output voltage magnitude and angular frequency command.

It should be noted that $P_{ci}$ and $Q_{ci}$ are not decoupled since the line impedance between $DG_i$ and PCC is complex. Different from most existing papers [11], [15], [18], [20], [21], where $P_{ci}$ and $Q_{ci}$ calculated with the sampled voltage of the filter capacitor and grid-side current are used in the droop equation (12), the virtual active power $P_i^{'}$ and reactive power $Q_i^{'}$ are preferred in this article. The difference between $P_{ci}Q_{ci}$ and $P_i^{'}Q_i^{'}$ is the power consumed by $Z_{oi}$ and $Z_{vi}$ which may not be negligible.

## III. Proposed $P - \dot{V}$ Droop Control Method

Since the virtual active power $P_i^{'}$ sharing accuracy is often degraded under the traditional methods owing to the mismatched feeder impedance, the following original and modified $P - \dot{V}$ droop control method are proposed to improve the active power-sharing accuracy.

### A. Original $P - \dot{V}$ Droop Control Method

In this section, a $P - \dot{V}$ droop control method is proposed, where $\dot{V}$ represents the time rate of change of the output voltage reference

$$\begin{aligned} \dot{V}_{oi} &= m_i(P_{oi}^{'} - P_i^{'}) \\ V_i &= V^* + \int_t \dot{V}_{oi}d\tau \end{aligned} \tag{13}$$

where $P_{oi}^{'}$ is the virtual active power set point at the nominal $V_i$, $\dot{V}_{oi}$ is the changing rate of $V_i$, and $V^* = 311$ V is the nominal voltage reference.

The operation of proposed $P - \dot{V}$ method is illustrated in Fig. 6. Supposing that the rated power of $DG_2$ is half of that of $DG_1$, then $P_{N1} = 2P_{N2}, m_2 = 2m_1$. At the beginning of operation time $t_0$, both the DGs are operated in steady state and the initial virtual active power is shared proportionally, $m_1P_1^{'}(t_0) = m_2P_2^{'}(t_0)$. As the loads increase at time $t_1$, the output power of $DG_1$ increases sharply to $P_1^{'}(t_1)$ to pick up the loads while that of $DG_2$ rises marginally to $P_2^{'}(t_1)$. Since

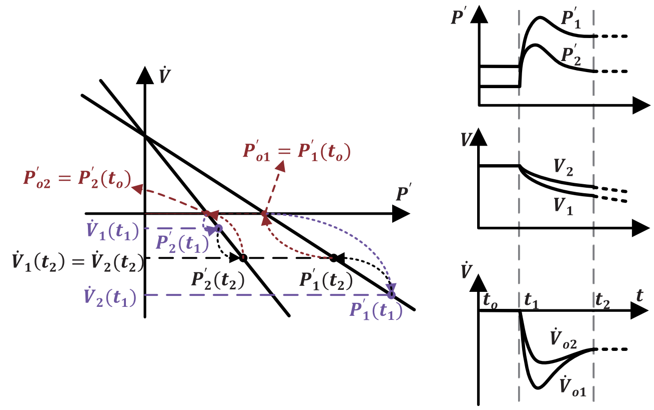

Fig. 6. Operation of proposed $P^{'}-\dot{V}$ droop controller.

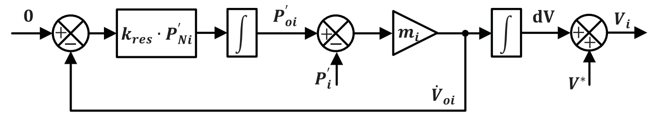


Fig. 7. Block diagram of the restoration mechanism.

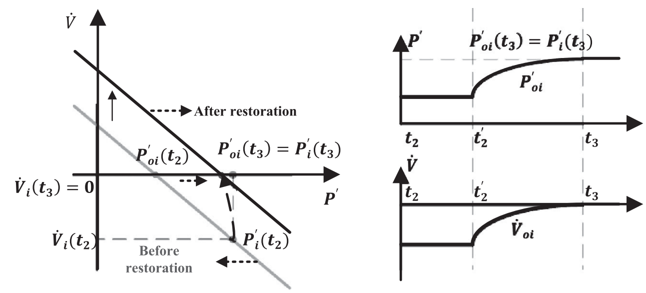


Fig. 8. Operation of $\dot{V}$ restoration process.

$P_1^{'}(t_1)$ is larger than $P_2^{'}(t_1)$, $\dot{V}_{o1}(t_1)$ is more negative than $\dot{V}_{o2}(t_1)$ according to proposed droop control equation (13). During the interval $t_1$ and $t_2$, both $\dot{V}_{o1}$ and $\dot{V}_{o2}$ decrease at first and then increase until they reach the balanced point $\dot{V}_{o1}=\dot{V}_{o2}$. The changing rate of $P_i^{'}$ is opposite to the case of $\dot{V}_{oi}$. The voltage magnitude reference decreases rapidly at the beginning and then slows down since $\dot{V}_{oi}$ increases.

At time $t_2$, the virtual active power $P^{'}$ has been shared proportionally and $\dot{V}_{o1}=\dot{V}_{o2}$. The resulting $V_1$ and $V_2$ decrease at the same pace without changing their relative magnitude. According to (13), the following equation holds: $m_1(P_1^{'}-P_{o1}^{'})=m_2(P_2^{'}-P_{o2}^{'})=\cdots m_n(P_n^{'}-P_{on}^{'})$. Considering the initial steady state at $t_0$, $m_1P_{o1}^{'}=m_2P_{o2}^{'}=\cdots m_nP_{on}^{'}$, then the virtual active power of each DG satisfies $m_1P_1^{'}=m_2P_2^{'}=\cdots m_nP_n^{'}$, which means the virtual active power has been shared proportionally.

It should be mentioned that $V_i$ and $P_i^{'}$ still decrease after time $t_2$ as long as $P_i^{'}\neq P_{oi}^{'}$. However, this tendency is neglected here since the following introduced restoration mechanism will force the $\dot{V}_{oi}$ to be zero.

## B. Restoration Mechanism

After $\dot{V}_{oi}$ reaches the balanced point, there must exist a restoration mechanism bringing $\dot{V}_{oi}$ back to zero to prevent the output magnitude varying. The $\dot{V}_i$ restoration mechanism is designed as follows:

$$\dot{P}_{oi}^{'}=-k_{\mathrm{res}}P_{Ni}^{'}\dot{V}_{oi} \tag{14}$$

where $k_{\mathrm{res}}$ is the restoration gain, $P_{Ni}^{'}$ is the rated virtual active power capacity, and $m_1P_{N1}^{'}=m_2P_{N2}^{'}=\cdots m_nP_{Nn}^{'}$.

Assuming that the time constant of the restoration control is much longer than that of $P-\dot{V}$ droop control the following relationship is derived:

$$\frac{d(\dot{V}_{oi})}{dt}=m_i\dot{P}_{oi}^{'}=-m_ik_{res}P_{Ni}^{'}\dot{V}_{oi}=-k_{res}^{'}\dot{V}_{oi} \tag{15}$$

where $k_{res}^{'}=m_ik_{res}P_{Ni}^{'}$.

The above equation shows that $\dot{V}_{oi}$ will exponentially decay to zero after the restoration mechanism is executed. With the same $k_{\mathrm{res}}$ adopted for different DGs, $\dot{V}_{oi}$ of different DGs will decay at the same pace.

The proposed $P-\dot{V}$ together with the restoration mechanism is illustrated as Fig. 7.

Fig. 8 demonstrates the operation of $\dot{V}$ restoration. Assuming that the restoration starts at time $t=t_2^{'}$, $\dot{V}_i$ and $P_{oi}^{'}$ hold the same value while $P_i^{'}$ decreases at the same pace due to the continuing reduction of voltage magnitude $V_i$ during $t_2$ and $t_2^{'}$. After $t_2^{'}$, the proposed restoration mechanism continuously drives $\dot{V}_{oi}$ to the 0 as can be observed in Fig. 7. At $t=t_3$, $\dot{V}_{oi}$ is reset to be zero and then $V_i$ keeps constant. During $t_2^{'}$ and $t_3$, the proposed restoration mechanism raises up $P_{oi}^{'}$ until it is equal to $P_i^{'}$. Comparing with $t=t_2^{'}$, $P_i^{'}(t_3)$ is slightly smaller than $P_i^{'}(t_2)$ owing to the continuing decrease of $V_i$ and the difference between them is affected by the convergence rate of the restoration mechanism. After $t=t_3$, the system has entered into the steady state.

It should be noted that both Fig. 6 and 8 only give the case of abrupt increase of loads. The opposite case can be analyzed accordingly and is omitted here.

## C. Modified $P-\dot{V}$ Droop Control Method

Although the original $P-\dot{V}$ droop method is able to improve the active power-sharing accuracy, its transient and steady performance can be further optimized. A modified $P-\dot{V}$ droop control method is proposed as follows, where the restoration mechanism remains the same:

$$\dot{V}_{oi}=m_i(P_{oi}^{'}-P_i^{'})$$

$$V_i=V^*+S_p\cdot\int_t\dot{V}_{oi}d\tau \tag{16}$$

where $S_p>1$ is a proportional coefficient and the difference between the original and modified $P-\dot{V}$ strategy will be compared in the following section.

## IV. Discussion on the Effects of Relative Coefficients

In this section, the effect of relative coefficients is discussed. According to (16), one can have

$$\frac{d\dot{V}_{oi}}{dt} = m_i(\dot{P}'_{oi} - \dot{P}'_i). \tag{17}$$

Considering the restoration mechanism (14), it can be transformed into

$$\frac{d\dot{V}_{oi}}{dt} = -m_i k_{res} P'_{Ni} \dot{V}_{oi} - m_i \dot{P}'_i. \tag{18}$$

The differential form of the $P'_i$ can be derived from (11)

$$\begin{aligned}\dot{P}'_i &= \frac{\dot{V}_i(V_i - V_o) + V_i(\dot{V}_i - \dot{V}_o)}{R'_{vi}} \\ &\approx \frac{2(1-k_i)V_i\dot{V}_i}{R'_{vi}}\end{aligned} \tag{19}$$

where $V_o$ is assumed to be proportional to $V_i, V_o \approx k_i V_i$.

With (16) and (19), one can have

$$\dot{P}'_i \approx \frac{2(1-k_i)V^*}{R'_{vi}} \cdot S_p \dot{V}_{oi} \tag{20}$$

where the actual voltage deviation $S_p \cdot \int \dot{V}_{oi} d\tau$ is smaller than allowed value $\delta V_{\max} = 0.05V^*$ and is thus ignored here. Combine (18) and (20)

$$\frac{d\dot{V}_{oi}}{dt} \approx -m_i \left( k_{\text{res}} P'_{Ni} + \frac{2(1-k_i)V^*}{R'_{vi}} \cdot S_p \right) \cdot \dot{V}_{oi}. \tag{21}$$

Thus, the convergency rate is

$$C_{\text{rmi}} = C_{\text{roi}} + \frac{2(1-k_i)V^*}{R'_{vi}} \cdot m_i S_p \tag{22}$$

where $C_{\text{roi}} = m_i k_{\text{res}} P'_{Ni}$ is the convergency rate of the original droop method (13).

Since the second term of (22) is positive, $C_{\text{rmi}}$ is larger than $C_{\text{roi}}$. Thus, the convergency rate of the modified droop method is faster than the original one and the difference between them can be adjusted by $k_{\text{res}}, S_p, m_i$, and $R'_{vi}$. Since $m_i$ and $R'_{vi}$ are predefined in this article, only $k_{\text{res}}$ and $S_p$ are discussed in this section.

The ultimate expression of $\dot{V}_{oi}$ is listed as follows:

$$\dot{V}_{oi}(t) = \dot{V}_{oi}(0) \cdot e^{-C_{\text{rmi}} \cdot t}. \tag{23}$$

The total voltage deviation whenever load changes can be calculated as

$$\begin{aligned}\delta V_{\text{roi}} &= 1 \cdot \int \dot{V}_{oi}(0) \cdot e^{-C_{\text{roi}} \cdot t} dt \\ &= \left(P'_{oi}(0) - P'_i(0)\right)\left(k_{\text{res}} P'_{Ni}\right)^{-1} \\ \delta V_{\text{rmi}} &= S_p \cdot \int \dot{V}_{oi}(0) \cdot e^{-C_{\text{rmi}} \cdot t} dt \\ &= \left(P'_{oi}(0) - P'_i(0)\right)\left(\frac{k_{\text{res}} P'_{Ni}}{S_p} + \frac{2(1-k_i)V^*}{R'_{vi}}\right)^{-1}\end{aligned} \tag{24}$$

where $P'_i(0)$ and $P'_{oi}(0)$ are the initial value and initial set point of virtual active power, respectively, when the load changes.

With $S_p = 5$ which are defined later, $k_{\text{res}} P'_{Ni} > \frac{k_{\text{res}} P'_{Ni}}{S_p} + \frac{(1-k_i)V^*}{R'_{vi}}$, thus $\delta V_{\text{roi}} < \delta V_{\text{rmi}}$, which means the total voltage deviation of the modified method is larger than the original one. However, as long as $\delta V_{\text{rmi}}$ is constrained in an allowable level, the modified droop method is preferred for its transient performance.

Apart from the convergency rate and voltage difference, the difference of $P'_{oi}$ between DGs is another indicator of the performance of the proposed droop method. According to (14), the steady state active power-sharing difference $\delta P'_{oio}$ of the original $P - \dot{V}$ method and $\delta P'_{oim}$ of the modified one are derived as follows:

$$\begin{aligned}\delta P'_{oio} &= \frac{P'_1(0) - P'_2(0) + \frac{2(1-k_i)V^*}{P'_N R'_v k_{res}} \left[P'_{01}(0) - P'_{02}(0)\right]}{1 + \frac{2(1-k_i)V^*}{P'_N R'_v k_{res}}} \\ \delta P'_{oim} &= \frac{P'_1(0) - P'_2(0) + \frac{2(1-k_i)V^* \cdot S_p}{P'_N R'_v k_{res}} \left[P'_{01}(0) - P'_{02}(0)\right]}{1 + \frac{2(1-k_i)V^* \cdot S_p}{P'_N R'_v k_{res}}}.\end{aligned} \tag{25}$$

With simple manipulation, it can be derived that if

$$P'_{01}(0) - P'_{02}(0) < P'_1(0) - P'_2(0) \tag{26}$$

holds, then, $\delta P'_{oim} < \delta P'_{oio}$. Since condition (26) is easier to be fulfilled when the load changes, the sharing accuracy of the modified droop method (16) is better than that of original method (13). In addition, if $P'_{01}(0) = P'_{02}(0)$, (25) can be simplified as

$$\begin{aligned}\delta P'_{oio} &= \frac{P'_1(0) - P'_2(0)}{1 + \frac{2(1-k_i)V^*}{P'_N R'_v} \cdot \frac{1}{k_{\text{res}}}} \\ \delta P'_{oim} &= \frac{P'_1(0) - P'_2(0)}{1 + \frac{2(1-k_i)V^*}{P'_N R'_v} \cdot \frac{S_p}{k_{\text{res}}}}.\end{aligned} \tag{27}$$

It is more clear that $\delta P'_{oim} < \delta P'_{oio}$ as long as $S_p > 1$. In fact, the original droop method (13) is a special case of the modified one (16).

*Remark 1:* Since droop coefficient $m_i$ is not included in (24) and (25), only the convergency rate of the restoration process will be affected by $m_i$. In other words, the voltage drop $\delta V$ and virtual active power-sharing accuracy $\delta P'_{oi}$ are immune to the variation of $m_i$.

*Remark 2:* $k_{\text{res}}$ and $S_p$ should be carefully designed to reach a compromise between $\delta V$ and $\delta P'_{oi}$. Considering all the three equations (22), (24), and (27), if $S_p$ keeps constant, the bigger the $k_{\text{res}}$ is, the faster the convergency rate $C_{\text{rmi}}$ will be. Besides, the total voltage difference $\delta V$ will be smaller at the expense of a larger $\delta P'_{oi}$, which means the active power-sharing accuracy is deteriorated. Let $k_{\text{res}}$ be constant, with the increasing of $S_p$, it is interesting that the speed of restoration process is faster and the active power-sharing accuracy is improved at the same time at the cost of larger $\delta V$.

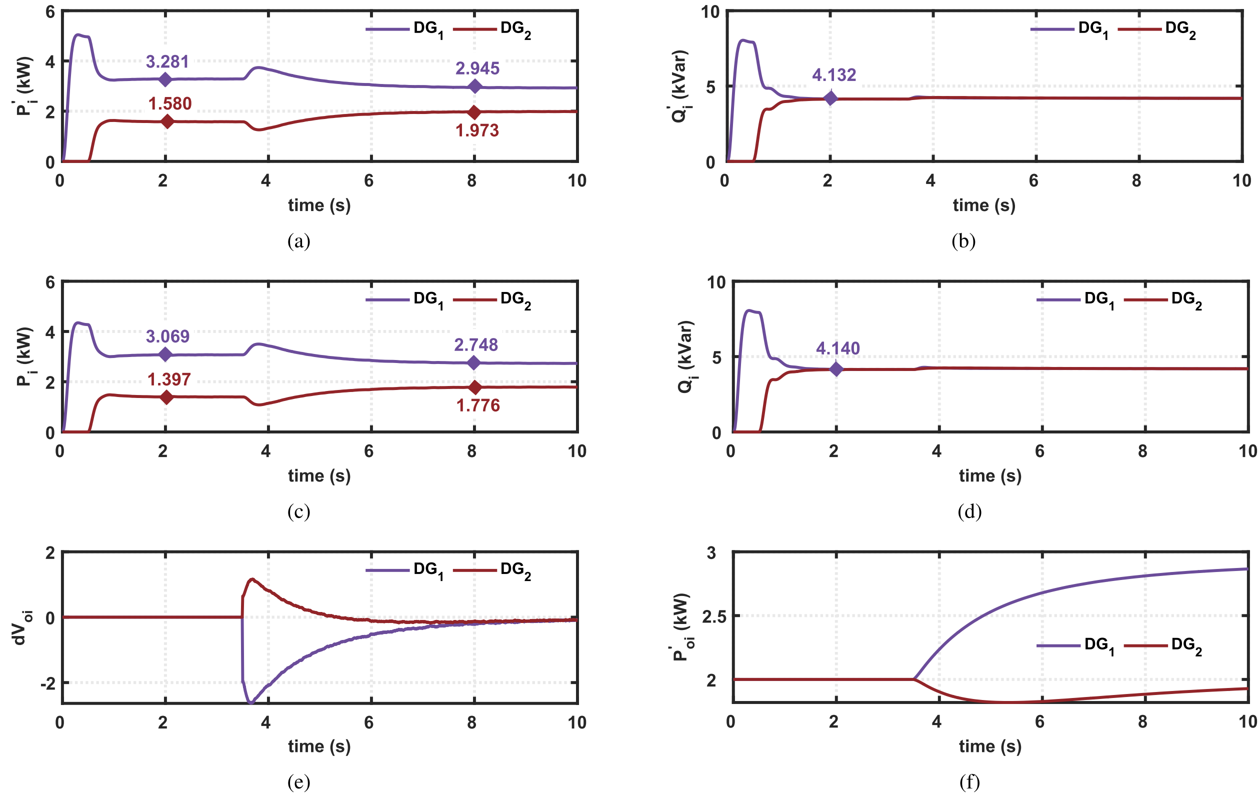


Fig. 9. Performance comparison of $P-V$ and $P-\dot{V}$ droop method. (a) Virtual active power $P'$. (b) Virtual reactive power $Q'$. (c) Injected active power $P$. (d) Injected reactive power $Q$. (e) Changing rate of $V_{oi}$. (f) Virtual active power Reference $P'_{oi}$.

To ensure the $\delta V_{\text{rmi}}$ is constrained in an acceptable level, the common code of 5% at most is adopted

$$\delta V_{\max} = \Delta P_{\max}\left(\frac{k_{\text{res}}P'_{Ni}}{S_p} + \frac{(1-k_i)V^*}{R'_{vi}}\right)^{-1} < 0.05V^*$$

$$\Rightarrow$$

$$\frac{k_{\text{res}}}{S_p} > \frac{20}{V^*} - \frac{2(1-k_i)V^*}{R'_{vi}P'_N} \approx \frac{20}{V^*} \approx 0.065. \tag{28}$$

In this study, the main consideration is the tradeoff between the voltage drop $\delta V$ and active power-sharing accuracy $\delta P'_{oi}$. With the instruction of Remark 2 and several experiments, $S_p = 5$ and $k_{\text{res}} = 0.325$ are adopted.

## V. Simulation Results

To verify the effectiveness of the proposed $P-\dot{V}$ method and the modified version, simulations based on MG of Fig. 1 is presented in Sections V-A and V-B. A complex MG case as shown in Fig. 11 is also analyzed in Section V-C. The line impedance and controller parameters of Fig. 1 are listed as follows.

1) The system voltage, frequency, switching frequency are $V^* = 311$ V, $f_0 = 50$ Hz, and $f_{sw} = 10$ kHz.
2) The converter-side and grid-side inductor, filter capacitor, and damping resistor are $L_{gi} = 1$ mH, $L_{oi} = 40$ uH, $C_i = 30$ uF, and $R_{ci} = 1.6\ \Omega$. The mismatched line impedance are $R_{L1} = 0.1\ \Omega$, $L_{L1} = 40$ uH, $R_{L2} = 0.3\,\Omega$, and $L_{L2} = 1$ mH.
3) The controller parameters are $K_p = 0.15, K_i = 200, K_I = 5.55$, and virtual resistor is $R_{vi} = 1\ \Omega$.

The different parameters of Fig. 11 compared with Fig. 1 are listed as follows.

1) The line impedance are $R_{12} = 0.1\ \Omega$, $L_{12} = 0.4$ mH, $R_{23} = 0.2\ \Omega$, $L_{23} = 0.6$ mH, $R_{34} = 0.4\ \Omega$, and $L_{34} = 0.8$ mH.

### A. Performance Comparison of P–V and $P-\dot{V}$ Droop Method

$DG_1$ starts at $t = 0$ s while $DG_2$ starts at $t = 0.2$ s and synchronizes with $DG_1$ through PLL. At $t = 0.5$ s, $DG_2$ is connected to PCC and both DGs are controlled under traditional $P-V$ droop method. The initial regulation process is deliberately presented in Fig. 9 and 10 for completeness.

Since the line impedance of DGs are different, it is obvious that the generated active power of DGs is unequal although their rated power is set to be same, which is the intrinsic flaw of traditional $P-V$ droop strategy [27].

Fig. 9(a) and (b) are the calculated virtual power while Fig. 9(c) and (d) are the power injected into PCC. It shows that the virtual power is larger than the injected power. For example, at $t = 2$ s, the injected active powers are $P_1 = 3069$ W, $P_2 = 1397$ W, while the virtual active powers are $P'_1 = 3281$ W, $P'_2 =$

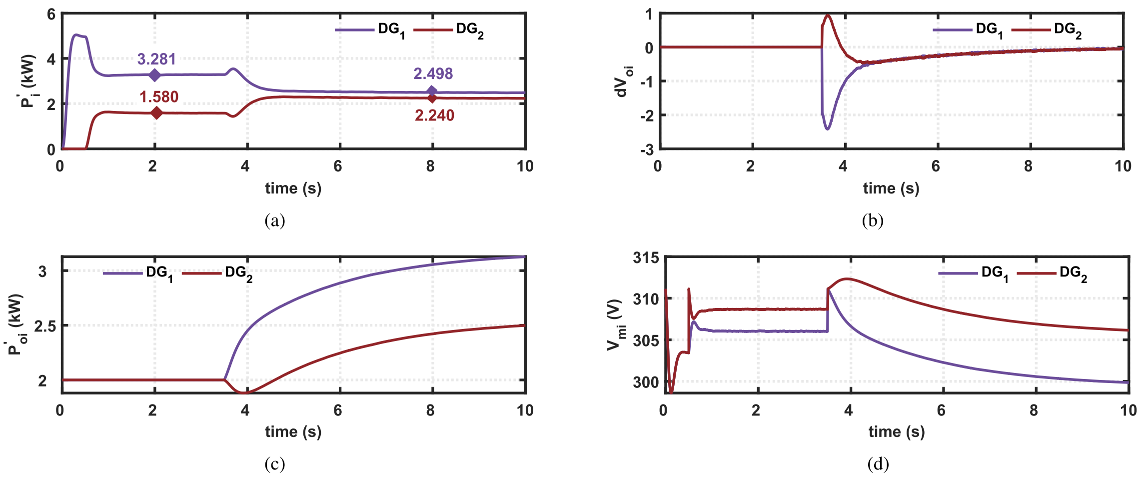


Fig. 10. Performance comparison of $P-V$ and modified $P-\dot{V}$ droop method. (a) Virtual active power $P^{'}$. (b) Changing rate of $V_{oi}$. (c) Virtual active power Reference $P^{'}_{oi}$. (d) Voltage magnitude $V_{mi}$.

1580 W. The injected reactive powers are $Q_1 = Q_2 = 4140$ Var while the virtual reactive powers are $Q_1^{'} = Q_2^{'} = 4132$ Var. This example verifies the opinion in Section II-C that the virtual power is different from the injected power and thus the decoupling of virtual power is not equal to the decoupling of injected power.

At $t = 3.5$ s, the proposed $P-\dot{V}$ droop method is activated. Compared with $t = 2$ s, the virtual active powers of DGs at $t = 8$ s are $P_1^{'} = 2945$ W, $P_2^{'} = 1973$ W. Thus, the active power-sharing has been improved from 48% at $t = 2$ s to 67% at $t = 8$ s. Besides, the reactive power is accurately shared among the regulation process.

According to Fig. 9(e), $\dot{V}_{oi}$ is zero before $t = 3.5$ s. After the $P-\dot{V}$ is activated, $\dot{V}_{oi}$ regulates the magnitude of voltage according to (13). After the initial dynamic regulation, $\dot{V}_{o1}$ and $\dot{V}_{o2}$ reach the same value and turn back to zero at the same pace. During the restoration process, the virtual active power reference $P^{'}_{oi}$ increases until $\dot{V}_{oi}$ reaches zero, as shown in Fig. 9(f). The difference between $P^{'}_{o1}$ and $P^{'}_{o2}$ is the root cause that the active power cannot be shared equally at the same power rating.

*Remark 3:* Before $t = 3.5$ s, the traditional droop equation (12) is adopted and the voltage reference $V_i$ deviates from its nominal value $V^*$. After $t = 3.5$ s, the droop method (12) is substituted by (13) and thus the initial voltage reference $V_i$ is equal to $V^*$ since the integral term is set to be zero initially. Therefore,there exists a sudden change of output power at $t = 3.5$ s as shown in Figs. 9 and 10.

## B. Improved Performance Brought by Modified Droop Method

As analyzed in Section IV, the transient performance of the modified $P-\dot{V}$ droop method can be improved with the proportional term $S_p$. With $S_p = 5$ and $k_{\text{res}} = 0.325$, the simulation result is presented in Fig. 10.

With the modified $P-\dot{V}$ droop method, the virtual active power-sharing accuracy at $t = 8$ s is 89%, which witnesses a 32% improvement compared with that in Fig. 9(a). The total time consumed before $\dot{V}_{oi}$ reaches the same value since $t = 3.5$ s in Fig. 10(b) is smaller than that of Fig. 9(e), which means that the transient performance of the modified method is better than that of the original one.

According to Fig. 10(c), the difference between $P^{'}_{o1}$ and $P^{'}_{o2}$ at steady state decreases compared with that of Fig. 9(f), which means the steady performance of the modified method is also improved compared to the original one. After the regulation process, the voltage level still satisfy the operation code which requires that 295 V $< V_{mi} <$ 326 V, as shown in Fig. 10(d) The above observation is consistent with Remark 2.

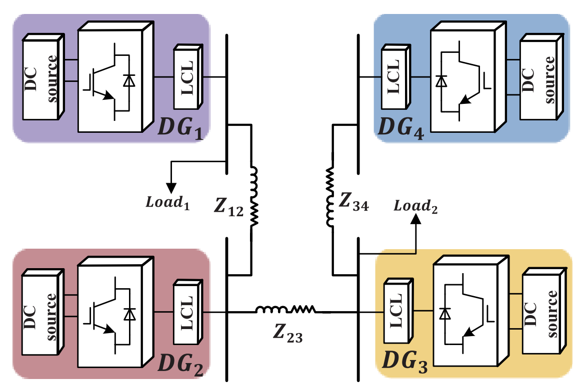


Fig. 11. Complex MG consists of four DGs and local loads.

## C. Performance Comparison Based on a Complex Microgrid

Thanks to the anonymous reviewer's advice, a complex microgrid as shown in Fig. 11 has been established in Matlab/Simulink. The starting process is the same as that in Sections V-A and V-B. In Fig. 12, the traditional $P-V$ droop method is utilized for the decentralized control of four DGs.

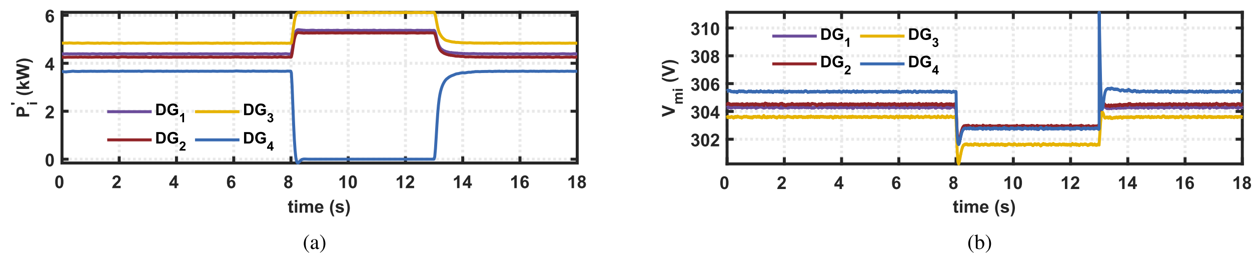


Fig. 12. Performance of $P-V$ droop method under a complex microgrid. (a) Virtual active power $P^{'}$. (b) Voltage magnitude $V_{mi}$.

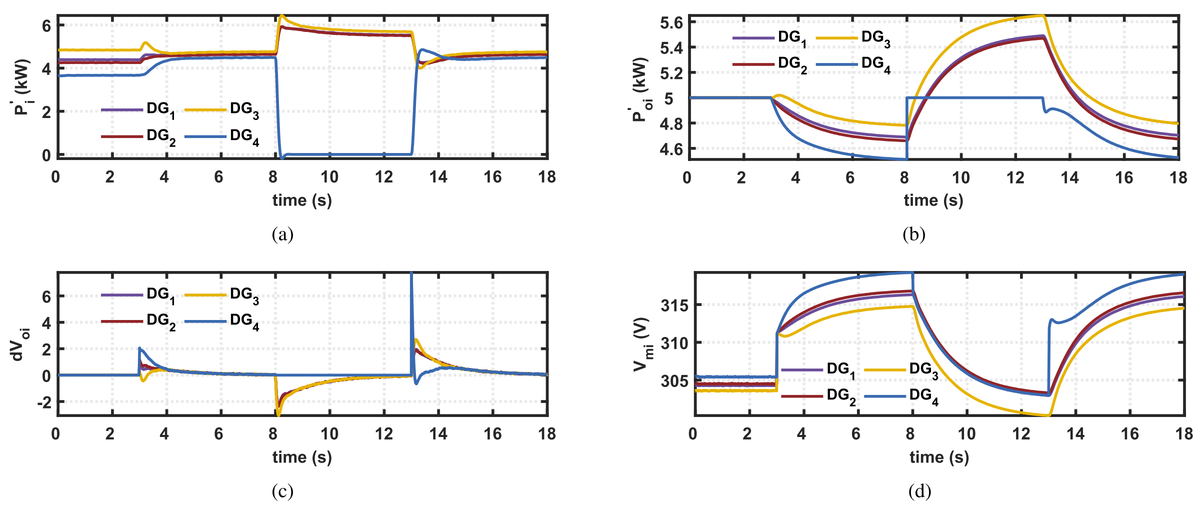


Fig. 13. Performance of modified $P-\dot{V}$ droop method under a complex microgrid. (a) Virtual active power $P^{'}$. (b) Virtual active power Reference $P_{oi}^{'}$. (c) Changing rate of $V_{oi}$. (d) Voltage magnitude $V_{mi}$.

The regulation process of the proposed modified $P-\dot{V}$ droop method is shown as Fig. 13.

To test the plug and play capability, $DG_4$ is disconnect from microgrid at $t = 8$ s and is reconnected at $t = 13$ s. In Fig. 13, the microgrid is controlled under $P-V$ droop method before $t = 3$ s, then it exchanges to the modified $P-\dot{V}$ droop method. Comparing Fig. 12(a) with Fig. 13(a), the active power-sharing accuracy of DGs has been apparently improved. The initial $P_{oi}^{'}$ is set to be 5 kW. Thus, when $DG_4$ is disconnected from MG, its value is reset to be 5 kW as shown in Fig. 13(b) during $8\text{ s} < t < 13$ s. Fig. 13(c) illustrates that whenever the load changes, $\dot{V}_{oi}$ will converge to a same value and then regulate the voltage at a same pace. During the whole regulation process, the voltage magnitudes satisfy that $295 < V_{mi} < 326$, as shown in Fig. 13(d). However, the voltage difference of Fig. 13(d) is slightly larger than that of Fig. 12(b), which is the cost of the improved active power-sharing accuracy.

In conclusion, the proposed modified $P-\dot{V}$ droop method still promise improved power-sharing accuracy under complex microgrid and is capable of dealing with plug and play incident.

## VI. Conclusion

In this article, a virtual positive resistor and negative inductor impedance strategy was adopted based on the analysis of the output impedance of DG in LVMG. With the equivalent impedance between VPS and PCC reshaped to be purely resistive, an original and a modified $P-\dot{V}$ droop methods were proposed to improve the active power-sharing accuracy, where the decoupled virtual power injected by VPS was adopted in droop equation rather than ordinary P/Q. A parameter $S_p$, which can accelerate the restoration process and reduce the sharing error at the same time, was incorporated in the modified $P-\dot{V}$ droop methods. Besides, the effect of $m_i$ and $k_{\text{res}}$ was also discussed. A simple MG consisting of two parallel DG with common load and a complex MG consisting of four DGs with local loads were constructed in MATLAB/Simulink. The simulation results demonstrated that the strategies proposed here were effective.

## References

[1] M. H. Rehmani, M. Reisslein, A. Rachedi, M. Erol-Kantarci, and M. Radenkovic, “Integrating renewable energy resources into the smart grid: Recent developments in information and communication technologies,” *IEEE Trans. Ind. Informat.*, vol. 14, no. 7, pp. 2814–2825, Jul. 2018.

[2] R. Bonetto, M. Rossi, S. Tomasin, and M. Zorzi, “On the interplay of distributed power loss reduction and communication in low voltage microgrids,” *IEEE Trans. Ind. Informat.*, vol. 12, no. 1, pp. 322–337, Feb. 2016.

[3] Z. Li, C. Zang, P. Zeng, H. Yu, and S. Li, “Fully distributed hierarchical control of parallel grid-supporting inverters in islanded ac microgrids,” *IEEE Trans. Ind. Informat.*, vol. 14, no. 2, pp. 679–690, Feb. 2018.

[4] J. Rocabert, A. Luna, F. Blaabjerg, and P. Rodríguez, "Control of power converters in AC microgrids," *IEEE Trans. Power Electron.*, vol. 27, no. 11, pp. 4734–4749, Nov. 2012.

[5] J. M. Guerrero, J. C. Vasquez, J. Matas, L. G. De Vicuna, and M. Castilla, "Hierarchical control of droop-controlled AC and DC microgrids—A general approach toward standardization," *IEEE Trans. Ind. Electron.*, vol. 58, no. 1, pp. 158–172, Jan. 2011.

[6] Y. Han, H. Li, P. Shen, E. A. A. Coelho, and J. M. Guerrero, "Review of active and reactive power sharing strategies in hierarchical controlled microgrids," *IEEE Trans. Power Electron.*, vol. 32, no. 3, pp. 2427–2451, Mar. 2017.

[7] M. N. Kabir, Y. Mishra, G. Ledwich, Z. Y. Dong, and K. P. Wong, "Coordinated control of grid-connected photovoltaic reactive power and battery energy storage systems to improve the voltage profile of a residential distribution feeder," *IEEE Trans. Ind. Informat.*, vol. 10, no. 2, pp. 967–977, May 2014.

[8] L. Ding, Q. Han, and X. Zhang, "Distributed secondary control for active power sharing and frequency regulation in islanded microgrids using an event-triggered communication mechanism," *IEEE Trans. Ind. Informat.*, vol. 15, no. 7, pp. 3910–3922, Jul. 2019.

[9] H. Xu, C. Yu, C. Liu, Q. Wang, F. Liu, and F. Li, "An improved virtual capacitor algorithm for reactive power sharing in multi-paralleled distributed generators," *IEEE Trans. Power Electron.*, vol. 34, no. 11, pp. 10 786–10 795, Nov. 2019.

[10] C. Dou, Z. Zhang, D. Yue, and M. Song, "Improved droop control based on virtual impedance and virtual power source in low-voltage microgrid," *IET Gener. Transmiss. Distribution*, vol. 11, no. 4, pp. 1046–1054, 2017.

[11] J. M. Guerrero, J. Matas, L. Garcia De Vicunagarcia De Vicuna, M. Castilla, and J. Miret, "Wireless-control strategy for parallel operation of distributed-generation inverters," *IEEE Trans. Ind. Electron.*, vol. 53, no. 5, pp. 1461–1470, Oct. 2006.

[12] J. He and Y. W. Li, "Analysis, design, and implementation of virtual impedance for power electronics interfaced distributed generation," *IEEE Trans. Ind. Appl.*, vol. 47, no. 6, pp. 2525–2538, Nov. 2011.

[13] J. He, Y. W. Li, and F. Blaabjerg, "An enhanced islanding microgrid reactive power, imbalance power, and harmonic power sharing scheme," *IEEE Trans. Power Electron.*, vol. 30, no. 6, pp. 3389–3401, Jun. 2015.

[14] R. An, Z. Liu, and J. Liu, "Modified adaptive virtual impedance method to compensate mismatched line impedances in microgrids," in *Proc. IEEE Appl. Power Electron. Conf. Expo.*, Mar. 2019, pp. 1109–1114.

[15] C. Lee, C. Chu, and P. Cheng, "A new droop control method for the autonomous operation of distributed energy resource interface converters," in *Proc. IEEE Energy Convers. Congr. Expo.*, Sep. 2010, pp. 702–709.

[16] J. Zhou and P. Cheng, "A modified $q - \dot{V}$ droop control for accurate reactive power sharing in distributed generation microgrid," *IEEE Trans. Ind. Appl.*, vol. 55, no. 4, pp. 4100–4109, Jul. 2019.

[17] A. Tuladhar, H. Jin, T. Unger, and K. Mauch, "Control of parallel inverters in distributed AC power systems with consideration of line impedance effect," *IEEE Trans. Ind. Appl.*, vol. 36, no. 1, pp. 131–138, Jan. 2000.

[18] J. He and Y. W. Li, "An enhanced microgrid load demand sharing strategy," *IEEE Trans. Power Electron.*, vol. 27, no. 9, pp. 3984–3995, Sep. 2012.

[19] B. Liu, Z. Liu, J. Liu, R. An, H. Zheng, and Y. Shi, "An adaptive virtual impedance control scheme based on small-AC-signal injection for unbalanced and harmonic power sharing in islanded microgrids," *IEEE Trans. Power Electron.*, vol. 34, no. 12, pp. 12 333–12 355, Dec. 2019.

[20] Q. Zhong, "Robust droop controller for accurate proportional load sharing among inverters operated in parallel," *IEEE Trans. Ind. Electron.*, vol. 60, no. 4, pp. 1281–1290, Apr. 2013.

[21] J. He, Y. W. Li, J. M. Guerrero, F. Blaabjerg, and J. C. Vasquez, "An islanding microgrid power sharing approach using enhanced virtual impedance control scheme," *IEEE Trans. Power Electron.*, vol. 28, no. 11, pp. 5272–5282, Nov. 2013.

[22] M. Kosari and S. H. Hosseinian, "Decentralized reactive power sharing and frequency restoration in islanded microgrid," *IEEE Trans. Power Syst.*, vol. 32, no. 4, pp. 2901–2912, Jul. 2017.

[23] Y. W. Li and C. Kao, "An accurate power control strategy for power-electronics-interfaced distributed generation units operating in a low-voltage multibus microgrid," *IEEE Trans. Power Electron.*, vol. 24, no. 12, pp. 2977–2988, Dec. 2009.

[24] H. Mahmood, D. Michaelson, and J. Jiang, "Accurate reactive power sharing in an islanded microgrid using adaptive virtual impedances," *IEEE Trans. Power Electron.*, vol. 30, no. 3, pp. 1605–1617, Mar. 2015.

[25] C. Lee, C. Chu, and P. Cheng, "A new droop control method for the autonomous operation of distributed energy resource interface converters," *IEEE Trans. Power Electron.*, vol. 28, no. 4, pp. 1980–1993, Apr. 2013.

[26] H. Han, X. Hou, J. Yang, J. Wu, M. Su, and J. M. Guerrero, "Review of power sharing control strategies for islanding operation of AC microgrids," *IEEE Trans. Smart Grid*, vol. 7, no. 1, pp. 200–215, Jan. 2016.

[27] J. M. Guerrero, J. Matas, L. Garcia de Vicuna, M. Castilla, and J. Miret, "Decentralized control for parallel operation of distributed generation inverters using resistive output impedance," *IEEE Trans. Ind. Electron.*, vol. 54, no. 2, pp. 994–1004, Apr. 2007.

[28] T. L. Vandoorn, J. D. M. De Kooning, B. Meersman, J. M. Guerrero, and L. Vandevelde, "Automatic power-sharing modification of $p/\,v$ droop controllers in low-voltage resistive microgrids," *IEEE Trans. Power Del.*, vol. 27, no. 4, pp. 2318–2325, Oct. 2012.

[29] A. G. Yepes, F. D. Freijedo, J. Doval-Gandoy, Ó. López, J. Malvar, and P. Fernandez-Comesaña, "Effects of discretization methods on the performance of resonant controllers," *IEEE Trans. Power Electron.*, vol. 25, no. 7, pp. 1692–1712, Jul. 2010.

[30] Y. Yang, K. Zhou, and M. Cheng, "Phase compensation resonant controller for PWM converters," *IEEE Trans. Ind. Informat.*, vol. 9, no. 2, pp. 957–964, May 2013.

[31] Y. Han, P. Shen, X. Zhao, and J. M. Guerrero, "Control strategies for islanded microgrid using enhanced hierarchical control structure with multiple current-loop damping schemes," *IEEE Trans. Smart Grid*, vol. 8, no. 3, pp. 1139–1153, May 2017.

[32] A. Eisapour-Moarref, M. Kalantar, and M. Esmaili, "Power sharing in hybrid microgrids using a harmonic-based multi-dimensional droop," *IEEE Trans. Ind. Informat.*, vol. 16, no. 1, pp. 109–119, Jan. 2020.

**Jianbo Chen** (Student Member, IEEE) received the B.S. degree in electrical engineering and automation from the School of Automation, Nanjing University of Posts and Telecommunications, Nanjing, China, in 2015, where he is currently working toward the Ph.D. degree in information acquisition and control.

His current research interests include distributed control, event-triggered control, parallel control of multiple inverters, and the power quality improvement of the microgrid.

**Dong Yue** (Senior Member, IEEE) received the Ph.D. degree in engineering from the South China University of Technology, Guangzhou, China, in 1995.

He is currently a Professor and Dean of the Institute of Advanced Technology and College of Automation & AI, Nanjing University of Posts and Telecommunications. He was the Associate Editor for the*Journal of the Franklin Institute* and *International Journal of Systems Sciences* and the Guest Editor of Special Issue on New Trends in Energy Internet: Artificial Intelligence-based Control, Network Security and Management. Up to now, he has authored or co-authored more than 250 papers in international journals and two books. He holds more than 50 patents. His current research interests include analysis and synthesis of networked control systems, multiagent systems, optimal control of power systems, and Internet of Things.

Prof. Yue served as the Associate Editor for IEEE INDUSTRIAL ELECTRONICS MAGAZINE, IEEE TRANSACTIONS ON INDUSTRIAL INFORMATICS, IEEE TRANSACTIONS ON SYSTEMS, MAN AND CYBERNETICS: SYSTEMS, IEEE TRANSACTIONS ON NEURAL NETWORKS AND LEARNING SYSTEMS and the Guest Editor for the IEEE TRANSACTIONS ON SYSTEMS, MAN, AND CYBERNETICS: SYSTEMS.

**Chunxia Dou** (Member, IEEE) received the B.S. and M.S. degrees in automation from Northeast Heavy Machinery Institute, Qiqihaer, China, in 1989 and 1994, respectively, and the Ph.D. degree in measurement technology and instrumentation from the Institute of Electrical Engineering, Yanshan University, Qinhuangdao, China, in 2005.

In 2010, she joined the Department of Engineering, Peking University, Beijing, China, where she was a Postdoctoral Fellow for two years. Since 2005, she has been a Professor with the Institute of Electrical Engineering, Yanshan University, and a Professor with the Institute of Advanced Technology, Nanjing University of Posts and Telecommunications, Nanjing, China. Her current research interests include multiagent-based control, event-triggered hybrid control, distributed coordinated control, and multimode switching control and their applications in power systems, microgrids, and smart grids.

**Lei Chen** (Student Member, IEEE) received the B.Eng. degree in automation from the Tongda College of Nanjing University of Posts and Telecommunications, Yangzhou, China, in 2016. He is currently working toward the Ph.D. degree at the College of Automation and College of Artificial Intelligence, Nanjing University of Posts and Telecommunications, Nanjing, China.

His current research interests include systems modeling, vulnerability analysis, defense protection, and application complex networks into research on cyber-physical power systems.

**Shengxuan Weng** received the B.S. degree in applied mathmatics from the School of Mathematics and Statistics, Huazhong University of Science and Technology, Wuhan, China, in 2009, and the Ph.D. degree in control science and engineering from the School of Automation, Huazhong University of Science and Technology, in 2014.

Since 2014, he has been with the Institute of Advanced Technology, Nanjing University of Posts and Telecommunications, Nanjing, China. His current research interests include distributed control, multiagent system, and control approach in microgrid and smart grid.

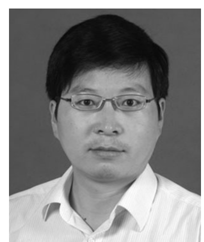

**Yanman LI** received the M.S. degree in cartography and geographic information system from Nanjing University, Nanjing, China, in 1996 and 1999.

He works as an Associate Professor Level Senior Engineer with the State Grid Electric Power Research Institute. His current research interests include distribution automation, active distribution network, and electric power automatic information system.